University of Oslo

FYS3150

Computational Physics

Modelling Contagion Dynamics

A Numerical Study of Deterministic and Stochastic Methods for the SIR Model

Authors
Lars Kristian Skaar
Håkon Lindholm
Brage Brevig
https://github.uio.no/lkskaar/FYS3150

December 17, 2020

1 Abstract

We evaluate the spread of disease in a network with the SIRS model. This is solved using the 4th order Runge-Kutta method, and Monte Carlo simulations. We start with a basic set of coupled differential equations, governed by rate of transmission, rate of recovery and rate of immunity loss. Later, more parameters are added to the model. This includes vital dynamics, seasonal variation of infection and vaccination. We wish to look at how the SIRS model can be used to model infectious diseases in the real world, and also survey the differences between a deterministic approach (Runge-Kutta) and stochastic one (Monte Carlo). We find that in many cases there is a good agreement between the two methods, but in some cases there is a large deviation, in which the stochastic simulation predicts an entirely different outcome than the deterministic approach. We study the effects of seasonal changes in the rate of transmission, and find that the networks arrive at an equilibrium, in which the total number of agents in each compartment fluctuates. The deterministic approach predicts a consistency in the peak numbers of infected agents, whilst the stochastic approach predicts a more realistic variation. A pulse vaccination strategy, being the most commonly used method to eradicate infection, is modeled and found to significantly reduce infection in the network over time. This is compared to a less realistic exponentially growing rate of vaccination, which dramatically reduces the number of infected agents when implemented.

Contents

2 Introduction

Just short of one year ago, the world first learnt of the Covid-19 virus, which has since then gone on to change the everyday life of people all around the globe. The family of coronaviruses (CoV) have been identified many times before, causing illnesses which may manifest themselves somewhere between the common cold and more severe disease. The introduction of a novel virus, however, calls for detailed studies of how different social and medical measures, alongside seasonal variation and vital dynamics have an impact on the short - and long term development of the number of infected agents within a network. The wording we devise in this article is deliberate, as this model does not only apply to human beings in a larger population, but also to other entities such as biological cells, or other non-sentient nodes in networks in which we may, as an example, study the communicable flow of information. This study is designed to develop a numerical model for the spread of contagious disease in a network of agents. To do this, we work via the SIRS[1] model and implement it numerically first through a set of coupled ordinary differential equations (ODEs), and later by a stochastic model in order to also capture the random nature of reality in our simulations. The stochastic modelling is in itself an interesting study, as the model may be applied in different areas of research such as information, rumor and substance addiction dynamics in a network. We will first go into detail on the SIR(S) model and its underlying assumptions, before we move on to explain how it may be numerically implemented, whether it is deterministically or stochastically. We shall then present select findings from our studies, and discuss them in light of both the numerical implementation and the effects of adding several layers of realism such as seasonal variation in rate of contagion and vaccination measures. Lastly, we make some summary remarks on the presented work.

[1] Susceptible - Infected - Recovered - Susceptible

3 Theory & Background

3.1 The SIRS Model

The SIRS model is a compartmental model describing the distribution of agents existing in each compartment

- Susceptible (S) - agents who are at risk of being infected by the disease,
- Infected (I) - agents who are infected by the disease and may pass on the disease to susceptible agents,
- Recovered (R) - agents who have recovered from the disease.

at a given time instance. It is a derivative of the simpler SIR model [1], including here the possibility of transitioning from the state of being 'removed' (recovered or deceased) into a state of being susceptible to future contagion.

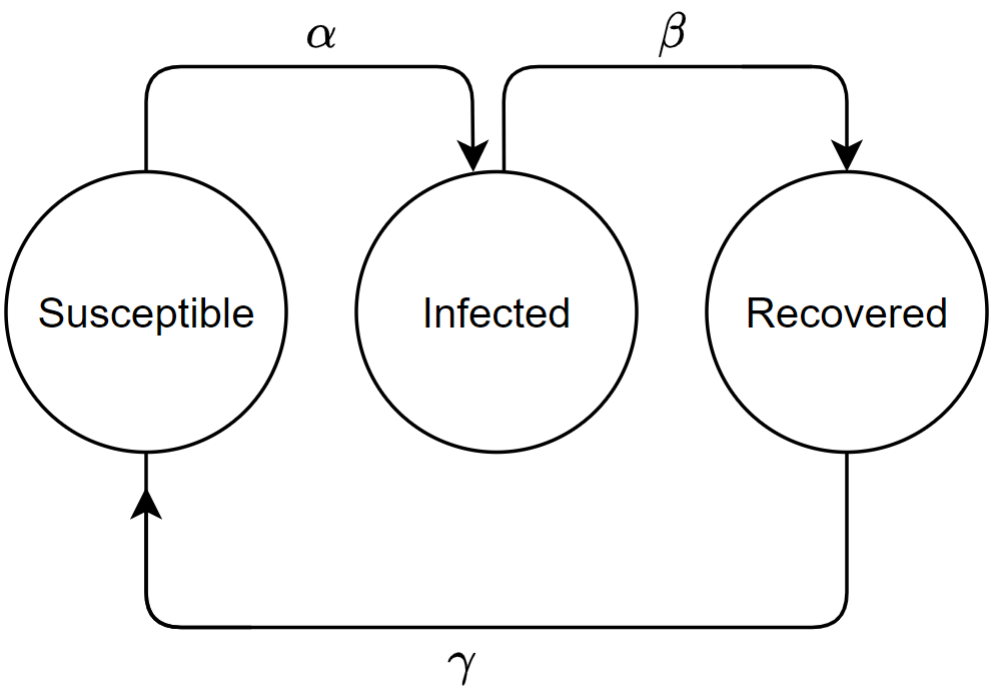

Figure 1: A modular flow chart describing how agents move between the three compartments S, I and R.

An agent may only transition between the network's compartments in a cyclic fashion as suggested by the model's name $S \xrightarrow{\alpha} I \xrightarrow{\beta} R \xrightarrow{\gamma} S$ with respective transition probabilities α, β and γ. The transmission

rate α, recovery rate β and immunity loss rate γ all have units of inverse time. As an example, setting $\alpha = \beta = \gamma = 1$ / day implies that the agents in the network on average contacts, recovers from and loses immunity to the disease within one day and may be taken as a measure of how long the agent exists in a given compartment. In the deterministic picture, we view the occupation of each compartment as a temporally continuous variable such that the dynamics of compartmental transition is governed by the following set of ordinary *non-linear*[2] differential equations

$$\begin{aligned} S'(t) &= \gamma R(t) - \alpha S(t) I(t)/N \\ I'(t) &= \alpha S(t) I(t)/N - \beta I(t) \\ R'(t) &= \beta I(t) - \gamma R(t) \end{aligned} \tag{1}$$

where $N = S(t) + I(t) + R(t)$ is the total number of agents in the network, and is for our simplest simulations assumed to be constant as we here omit vital dynamics considerations such as birth rate and natural death rate, assuming then that disease evolves in the network on a time scale which is significantly shorter than the time scale spanning the average agent's lifetime. In the stochastic picture, however, we first observe that for a sufficiently small temporal step Δt, at most one agent moves from a given compartment to another. As

$$\begin{cases} \max\{\underbrace{\alpha S I \Delta t/N}_{S\to I}\} = \alpha N \Delta t/4 \\ \max\{\underbrace{\beta I \Delta t}_{I\to R}\} = \beta N \Delta t \\ \max\{\underbrace{\gamma R \Delta t}_{R\to S}\} = \gamma N \Delta t \end{cases}$$

we may require that $\Delta t = \min\{4/\alpha N, 1/\beta N, 1/\gamma N\}$ and reinterpret

$$\begin{cases} P(S \to I) = \alpha S I \Delta t/N \\ P(I \to R) = \beta I \Delta t \\ P(R \to S) = \gamma R \Delta t \end{cases}$$

as transition probabilities. In this way, we may implement the SIRS model stochastically by generating (pseudo)random numbers and at each time step allow agents to move in and out of each compartment

[2] This implicates sensitivity to initial conditions.

by proposing transitions and either accepting or rejecting them by measuring each transition probability against the random numbers. It should be duly noted that the SIRS model further works on the basis of the following assumptions

- The population mixes homogeneously, id est every agent in the network is at all times equally likely to contact, recover and lose immunity to the disease.
- Following the homogeneity of the population, all the parameters describing transitions are averages.
- The disease has no pertaining incubation time. It is instantly transmitted, and those who contact the disease are immediately moved into compartment I.
- In the case of adding vital dynamics to the model, we assume that all newborns are initially susceptible.

3.2 Improving the Model

In this section we shall explore in what ways we may incorporate different realizations of the SIRS model in order to better capture the true nature of how infectious diseases may spread within a network. The layers of realism we add to the model in this project do not confer the possibility of making real - world predictions for the current, or any other, pandemic as this is a system with very complex behaviour in both temporal and spatial dimensions. Rather, it allows us to heuristically study their impact on the model.

In a first attempt of improving the model, we add the realization of vital dynamics across all compartments S, I and R. In many cases, the stages of identification, outbreak and eradication of an infectious disease may all occur within a time span significantly shorter than the average lifetime of the agents within the network. However, in a few select cases, this is far from the truth. A few examples include the Ugandan trypanosomiasis epidemic (1900 - 1920)[2], the HIV/AIDS pandemic (1981 - present) and the Antonine Plague (165 - 180, Roman Empire)[3]. Such long lasting diseases not only claim the lives of a significant percentage of the population, but their dynamics are also dependent on the in - and outflow of agents within the network. An improved modular scheme may be visualized as

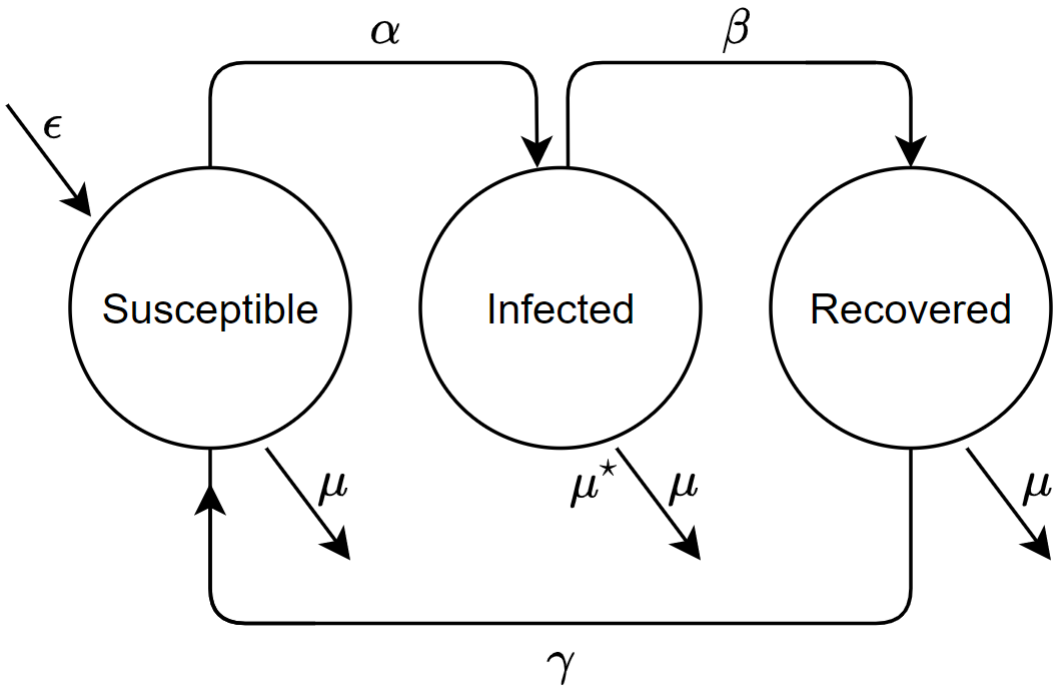

Figure 2: A modular flow chart describing the motion of agents between the compartments $S,\ I$ and R, now adding vital dynamics.

where $\mu,\ \mu^\star$ and ϵ denote the average death rate due to natural causes, the death rate due to the infectious disease and the average birth rate respectively. In the deterministic picture, we may construct a new set of differential equations

$$\begin{aligned} S'(t) &= \gamma R(t) - \alpha S(t) I(t)/N(t) - \mu S(t) + \epsilon N(t) \\ I'(t) &= \alpha S(t) I(t)/N(t) - \beta I(t) - (\mu + \mu^\star) I(t) \\ R'(t) &= \beta I(t) - \gamma R(t) - \mu R(t) \end{aligned} \tag{2}$$

where we now let the total number of agents in the network $N(t)$ be a continuous variable in time. For the stochastic simulation, we determine the temporal resolution Δt in the same way as before, now adding the possible transitions $S \to D,\ I \to D$ and $R \to D$ for a new compartment D in which deceased agents are moved to, $I \to D_I$ for a new compartment D_I in which agents who die from the disease are moved to, and $B \to S$ for a new compartment B in which newborns are moved from. As before, we may then

reconstruct new transition probabilities

$$\begin{cases} P(S \to D) = \mu S \Delta t \\ P(I \to D) = \mu I \Delta t \\ P(R \to D) = \mu R \Delta t \\ P(I \to D_I) = \mu^\star I \Delta t \\ P(B \to S) = \epsilon N \Delta t \end{cases}$$

As before, the vital dynamics realization will not allow us to make predictions of real - world statistical value, and now mainly because the provided examples of long lasting diseases are very complex in their transmission. HIV/AIDS is vertically transmitted, meaning that offspring are born with the disease, and the two other confer vector transmission, meaning that the disease is transmitted from animal carriers onto agents. Although we do not attempt to implement these conditions in this project, the additional layer of vital dynamics allow us to study the effect of death and birth in combination with the disease.

Many infectious diseases, after an initial outbreak, may after some time be categorized as an endemic disease. In this stage, the disease has strongly manifested at an non-zero equilibrium, around which the number of currently infected agents may fluctuate. Such fluctuations are largely conferred by seasonally variable transmission rates, and is the case for diseases like the 'flu' or measles. The variations themselves are to this day studied in detail as they are not fully understood, although the commonly accepted explanations are characteristic pathogen survival outside of host, and the behaviour of susceptible hosts[4][5]. Pathogens like the rota - and noroviruses, causing the 'flu', survive in cold climates unlike many other pathogens, and therefore display annual peaks in infection rates during the colder months of the year. Similarly, measles are a common disease among children, and analysis shows that there is a strong correlation between the rate of infection and the conglomeration of children at school, after - school activities and the alike, pertaining seasonal variation in transmission rates to the behavioural pattern of the pathogen's host. To model this realization in our program, we define the transmission rate as a function of time by

$$\alpha(t) = A\cos(\omega t) + \alpha_0 \tag{3}$$

in which α_0 is the average transmission rate, A is the amplitude of the variation, being the largest deviation from the average transmission rate, and ω denotes the frequency at which the transmission rate

changes. A flow chart describing the dynamics now adding seasonal variation may be taken as Figure 2, substituting α for $\alpha(t)$.

In a last attempt to make our model more realistic, we study the effects of vaccination, too. Vaccination is a powerful tool, and in many cases absolutely necessary in order to eradicate a disease in a network. This works by breaking the cyclic nature of the SIRS model, as agents in the susceptible state may be vaccinated and move directly into the recovered state. Agents in the recovered state may be vaccinated such that their possibility of moving into the state of being susceptible becomes zero.

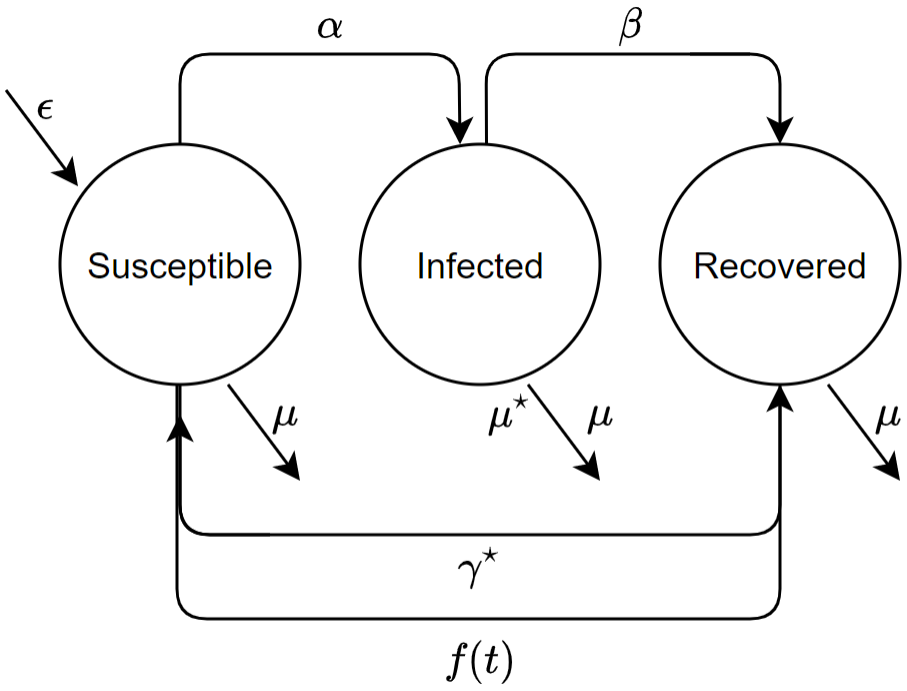

Figure 3: A final, compound modular flow chart describing all realizations of the SIRS model we have implemented.

Figure 3 describes the motion of agents in and out of the three different compartments, now having added the possibility of being vaccinated. This gives rise to $\gamma^\star$, still describing the rate of loss of immunity to the disease, but now only being applicable to agents occupying R whilst not having been vaccinated.

For the deterministic approach, a new set of coupled differential equations emerges as

$$
\begin{aligned}
S'(t) &= \gamma R(t) - \alpha S(t) I(t)/N - f(t) \\
I'(t) &= \alpha S(t) I(t)/N - \beta I(t) \\
R'(t) &= \beta I(t) - \gamma R(t) + f(t)
\end{aligned} \tag{4}
$$

in which $f(t)$ describes how the rate of vaccination varies with time. It may also be taken as a constant rate. For the stochastic approach, the only change needed in our program is the added transition probability $P(S \to R) = f(t)\Delta t$.

In this project we study two possible vaccination programs, one in which the agents in the network are continuously vaccinated by $f(t) = \exp(\delta t)$ for some constant δ as to realize the continuous development of vaccines and their exponentially growing availability. This is of course a highly idealized scenario as this is economically infeasible and rarely occurs. In the second attempt to realize a more common vaccination strategy, we add a rate of vaccination following

$$
f(t) = \begin{cases} \eta t, & \text{if } \cos(t) > 0 \\ 0, & \text{else} \end{cases} \tag{5}
$$

where $\eta \in \mathbb{R}$. This implementation is meant to simulate pulse vaccination, in which select groups within a network (children, elderly) are vaccinated at regular intervals as a mean of eradicating a disease. As our implementation of the SIRS model does not differentiate between agents (homogeneous mixing), we may still choose to vaccinate a given percentage of the occupants of the Susceptible compartment. Although pulse vaccination programs, such as the Pulse Polio Programme in India are well established, the mathematical and numerical aspects are still in their infancy which is why we find it necessary to study the effects of such a realization, too. Even though the pulse functions devised in other numerical and/or mathematical research papers are more formalized than the one we have chosen to implement, equation 5 severs its purpose as a mathematical pulse, and is in addition very easy to reformulate[3].

[3] As an example, we studied regular non-increasing pulses, for which equation 5 returns a constant.

3.3 Initial Conditions, Equilibrium and Stability

In this project we study four different networks

	A	B	C	D
α	4.0	4.0	4.0	4.0
β	1.0	2.0	3.0	4.0
γ	0.5	0.5	0.5	0.5

Table 1: The transition rates for the four different networks we study.

In all four networks, each compartment is initialized as $S_0 = 300$, $I_0 = 100$ and $R_0 = 0$. Upon adding different layers of realistic improvements to our model, we have devised many different initial conditions, all of which will be specified in the presented results.

The set of equations (2) define a conservative system as the population remains constant under the assumption that we may omit vital dynamics in the first place. By that, we eventually reach an equilibrium state $(S_\infty, I_\infty, R_\infty)$ for which it is possible to derive analytical values for the fraction of occupants in each compartment by setting each derivative equal to zero. We rather choose to give the total number of occupants in each compartment at equilibrium by

$$\begin{aligned} S_\infty &= N\frac{\beta}{\alpha} \\ I_\infty &= \frac{N(1-\frac{\beta}{\alpha})}{1+\beta\gamma} \\ R_\infty &= \frac{N\beta}{\gamma}\frac{1-\frac{\beta}{\alpha}}{1+\frac{\beta}{\gamma}} \end{aligned} \tag{6}$$

Notice in (6) that for any values of α and β such that $\beta < \alpha$, the number of infected agents at equilibrium is non - zero. In this project we only study the effect of varying the rate of recovery β in the simple SIRS model, mainly because this variable is more easily controllable by real - world health measures. It should be noted however, that the rate of transmission, or contact rate, is to some extent also controllable by imposing social measures such as wearing masks, increasing the availability of disinfectants or city-wide lockdown. We have not studied this parameter in detail as of now, as we rather would control this variable in a model which takes heterogeneous mixing into account, and is therefore a prospect for our future selves.

4 Numerical Methods and Implementation

4.1 The Runge - Kutta Method

As we saw in 3.1, we may develop a numerical SIRS model by taking $S(t),\ I(t)$ and $R(t)$ to be continuous variables in time, leading to the set of coupled differential equations (2). By solving each differential equation we obtain numerical solutions describing the temporal development of the number of agents existing in each compartment for an arbitrary simulation period. In order to solve (2) numerically, we devise a Runge - Kutta method of fourth order (RK4) as this solver commits a global error of $\mathcal{O}(h^4)$ for a given temporal resolution h. In our simulations, we have adapted temporal resolutions in the range of $10^{-2} - 10^{-3}$, committing very small global errors in order of $\mathcal{O}(10^{-8}) - \mathcal{O}(10^{-12})$. The RK4 method, like many other numerical integrators, solves differential equations by approximating the slope of the unknown solution $y(t)$ on partitioned[4] intervals $(t_n, t_n + \Delta t)$, for which Δt may be taken as h in our case. The approximation is made by weighting an average gradient in this interval by determining incremental gradients k_1, k_2, k_3 and k_4 at three temporal increments of $(t_n, t_n + h)$ in the following procedure

Computation of Incremental Gradients:

- Compute $k_1^{(n)} = f(t_n, y_n)$
- Compute $k_2^{(n)} = f(t_n + h/2, y_n + hk_1/2)$
- Compute $k_3^{(n)} = f(t_n + h/2, y_n + hk_2/2)$
- Lastly, compute $k_4^{(n)} = f(t_n + h, y_n + hk_3)$
- Update the solution by $y_{n+1} = y_n + (1/6)(k_1 + 2(k_2 + k_3) + k_4)$ and the current time by $t_{n+1} = t_n + h$

where $k_i^{(n)}$ denotes the incremental gradients k_i belonging to a solution y_n on the interval $(t_n, t_n + h)$. With Procedure 4.1 in place, a recipe for our numerical implementation of follows

[4] Partitions of the interval (t_0, t_f) for some finite simulation time t_f.

RK4 Algorithm for SIRS Model:

1. Initialize two vectors $\mathcal{S},\ \mathcal{D} \in \mathbb{R}^3$ in which we store the global solutions $S,\ I$ and R and derivatives $f(t_n, S_n),\ g(t_n, I_n)$ and $h(t_n, R_n)$ respectively with $S_0,\ I_0,\ R_0$ and t_0.
2. Pass the vectors to a function `RK4()`
3. Within the function `RK4()`, initialize local vectors $\mathcal{K}_1,\ \mathcal{K}_2,\ \mathcal{K}_3,\ \mathcal{K}_4,\ \mathcal{Y} \in \mathbb{R}^3$ in which we store the incremental gradients $k_i^{(n)}$ and local solutions $S_n,\ I_n$ and R_n
4. Loop through the local vectors in order to compute all incremental gradients and local solutions, finally updating the global solutions.

4.2 Random Sampling - Dynamical Monte Carlo Simulation

In the previous section, we explained in what way the RK4 method may be implemented in order to study the SIRS model. Solving the set of differential equations in (2) serves the purpose of deterministically computing the fraction of agents in each compartment at every time point. What we mean by this is that every updated solution is entirely dependent on the previous solution, and more importantly that, given the same initial conditions, the model will always return the same values. The model becomes flawed in the sense that it fails to capture the random nature of reality. To remedy this flaw, we implement a stochastic method for a Monte Carlo simulation of how an infectious disease spreads within a network. This implementation allows for simulations which deviate greatly from the deterministic model, and by that opens up for greater statistical interpretation of the model. By performing more and more simulations, we may also compute the expected temporal state evolution

Numerical Recipe for Stochastic Simulation of SIRS Model:

1. Initialize a vector $\mathcal{S}$ in which we store the states $S,\ I$ and R in each temporal step.
2. Calculate $\Delta t = \min\{T_1, T_2, \dots, T_n\}$ for the n different state transitions.
3. Calculate the respective transition probabilities $P(i \to j) = T_i \Delta t,\ \text{for } i = 1, 2, 3, \dots, n$
4. Generate a random number r, and measure it against all state transition probabilities.

   If $r < P(i \to j)$, accept the proposal and update the states $i, j \in \mathcal{S}$ by ± 1 depending on the transition type and move onto the next possible state transition. Else, reject the proposal and move onto the next possible state transition.
5. When all possible state transitions have been tested, the current time and state vector may be passed to a file for plotting purposes. The current time is in this step updated by dt.
6. Repeat steps 3-5.
7. Repeat steps 1-6 for a given number of simulations/experiments. In each simulation, pass every state vector to a list at each time point in order to find the average state vector at each time point.

4.2.1 Remarks on the Computation of Δt

In Sections 3.1 and 3.2 we explained in what way the temporal resolution Δt is computed in our program in order to ensure sufficiently small time steps for which we may realistically sample transitions made by a single agent in the network. However, in the case of improving the basic SIRS model, this computation may lead to dynamical computation of a time-dependent $\Delta t(t)$ as the network size $N(t)$ may vary greatly, as the seasonally variant transmission rate $\alpha(t)$ is introduced, or when the temporally variant vaccination function $f(t)$ is implemented. The fact that the time it takes for a possible transition to occur varies is actually an extra improvement on the Monte Carlo simulation itself, but we have chosen to fixate Δt in each simulation as varying the temporal resolution causes each simulation to have a different number of temporal points. This in turn makes it difficult to create sensible averages at each time point, as one would have to extrapolate averages between a set of time points within a given range. We have chosen not to do this in our project, as fixating Δt in each simulation produces interesting results in the first place.

4.2.2 Remarks on the Implementation of the Vaccination Function $f(t)$

When implementing the vaccination function, we encounter a problem with the homogeneous population assumption for the SIRS model. This assumption hinders us in keeping track of the health status of the 'individual' agents existing in R, as the concept of individuality is non-existent in this model. Each agent may have transitioned into R by either vaccination or by recovery from the disease, and without a proper implementation of individual health status IDs for each agent, it becomes possible for vaccinated agents to transition into S. In order to account for this issue we implement a new rate of loss of immunity γ which, for every agent transitioning into R by vaccination, updates by

$$\gamma(t + \Delta t) = \gamma(t) - \frac{\gamma(t)}{2N}$$

In this way, it becomes less and less likely for agents in R to transition back into S, following the evolution of agents moving directly from S to R. In another attempt to more rigorously remedy the lacking health status ID issue, we initialized a fourth compartment R_{TOT} in which we stored the total number of recovered agents. In this way, vaccinated agents in S moved directly to R_{TOT}, whilst recovered agents moved from I to R with the possibility of transitioning back into S. In this way, there is no need to change the rate of loss of immunity. However, as this caused us to run into issues with the plotting and representation of the data for the larger compound simulations (see Appendix A), we stuck to the first method described in this section.

5 Results

Table 2: Run times for MC method and RK4 method with 10^5 integration points and 30 stochastic simulations

Simulation Time	Average MC [s]	All MC [s]	RK4 [s]
10	0.0998	2.996	1.721
100	0.978	29.351	1.779
1000	10.182	305.479	1.723

Computational execution times for the program is presented in Table 2. "Average MC" shows the average time for each Monte Carlo simulation across 30 simulations, while "All MC" pertains to the total time for all 100 simulations. As can plainly be seen from the table, while the computational time for the average Monte Carlo simulation increases linearly, the Runge-Kutta solver is more or less constant for admittedly pretty short simulations. Simulations with times beyond 1000 are unnecessary to show here,

as the differences between Monte Carlo and Runge-Kutta are obvious.

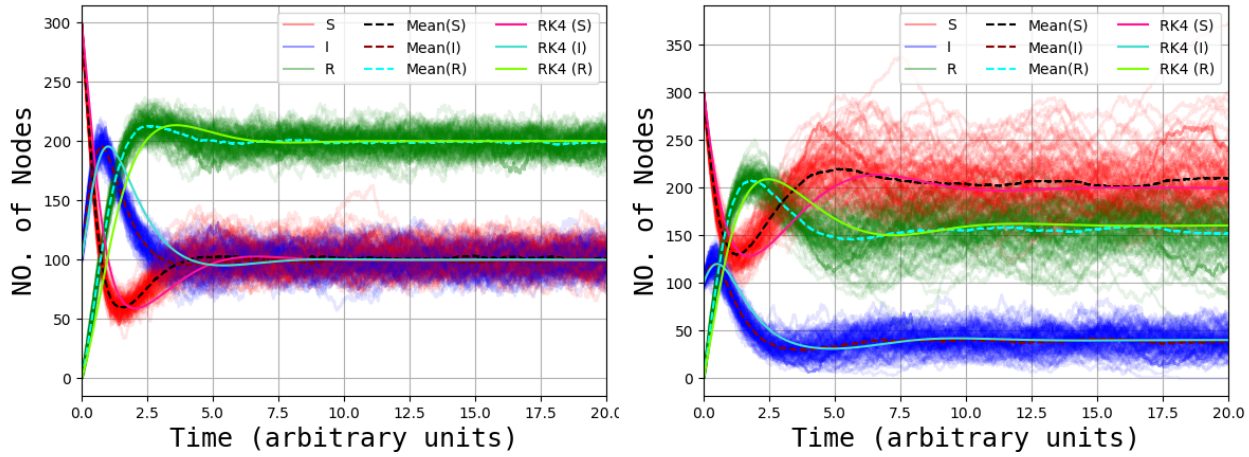

(a) $\beta = 1$ (b) $\beta = 2$

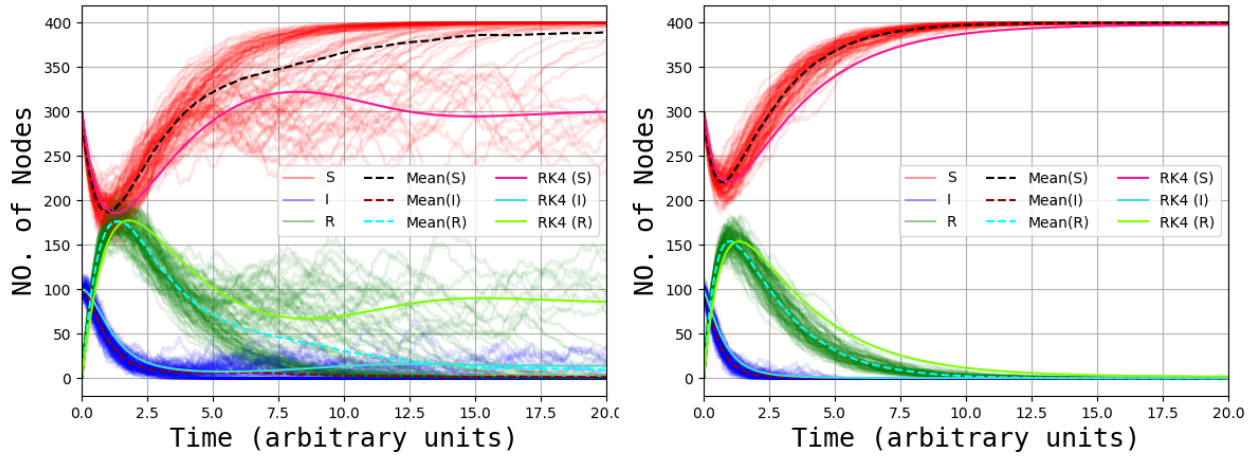

(c) $\beta = 3$ (d) $\beta = 4$

Figure 4: Temporal development of the S, I and R populations, with different initial value for β, the rate of recovery. $\alpha = 4$ and $\gamma = 0.5$

The four plots in Figure 4 shows the development of the populations of S, I and R with time with different values of β for each plot. The values for α and γ are held constant. For each plot, the Monte Carlo simulation has been run 100 times. These are the fine red, green and blue lines with varying degree of hue seen in the plots. This allows a deeper shade of color to be interpreted as statistically more common outcomes. The dashed lines show the expectation values at each point in time between all the simulations. The solid lines correspond to the Runge-Kutta solutions.

S				
β	1	2	3	4
S_∞	100	200	300	400
RK4	99.75	199.90	300.24	397.80
MC	101.94	207.51	380.68	399.98

I				
β	1	2	3	4
I_∞	100	40	14.28	0
RK4	100.08	40.07	14.06	0.21
MC	98.21	37.22	1.98	0.0

R				
β	1	2	3	4
R_∞	200	160	85.71	0
RK4	200.17	160.03	85.70	1.99
MC	199.85	155.27	17.34	0.02

Table 3: Expectation values for Monte Carlo simulations after equilibration. The final corresponding Runge-Kutta value, and the fraction of people in each population at equilibrium, for each value of β.

Table 3 shows the total number of agents occupying each compartment at equilibrium for each of the four different networks as computed by the expressions in (6). This is compared to the final value from the plots in Figure 4, where "RK4" is the value obtained from the Runge-Kutta solver, and "MC" is the expectation value acquired across all 100 simulations.

β	S		I		R	
	σ	$\bar{x}$	σ	$\bar{x}$	σ	$\bar{x}$
1	11.62	101.94	12.39	98.21	9.30	199.85
2	29.70	207.51	13.02	37.22	1.99	155.27
3	23.96	380.68	3.22	1.98	21.29	17.34
4	0.14	399.98	0.0	0.0	0.14	0.02

Table 4: Expectation values $\bar{x}$ and standard deviations σ for the Monte Carlo simulations after equilibrium.

Table 4 shows the expectation values across 100 Monte Carlo simulations at equilibrium as well as the standard deviation, for varying values of β.

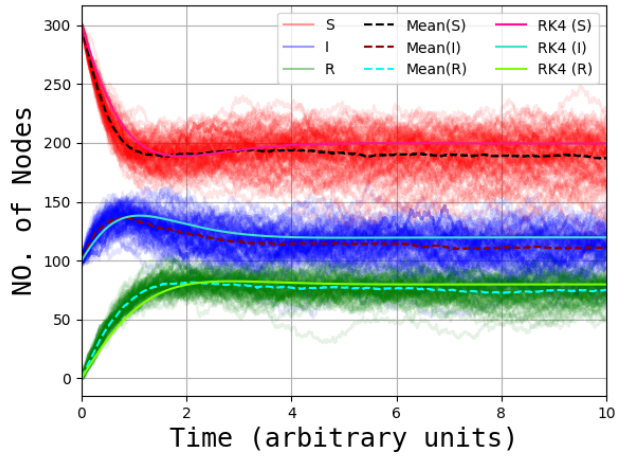

(a) $\alpha = 4$, $\beta = 1$, $\gamma = 0.5$, $\mu = 1$, $\mu^* = 0$, $\epsilon = 1$

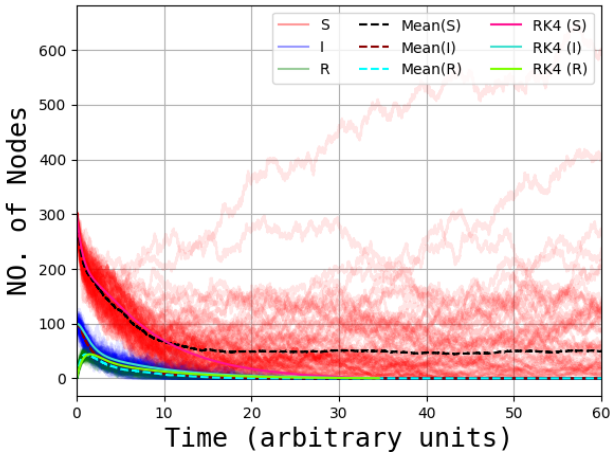

(b) $\alpha = 4$, $\beta = 1$, $\gamma = 0.5$, $\mu = 1$, $\mu^* = 1$, $\epsilon = 1$

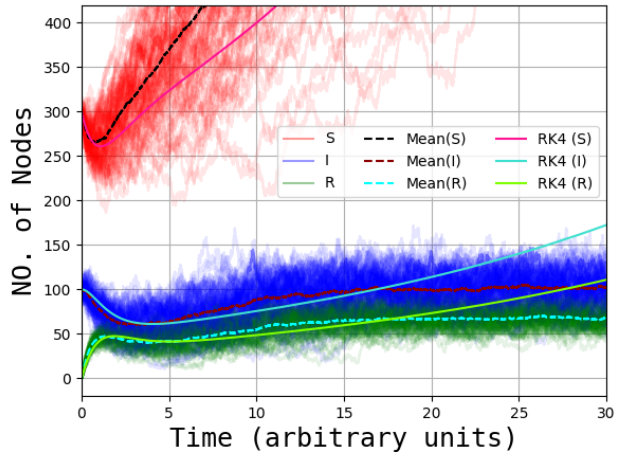

(c) $\alpha = 4$, $\beta = 1$, $\gamma = 0.5$, $\mu = 1$, $\mu^* = 1$, $\epsilon = 1.2$

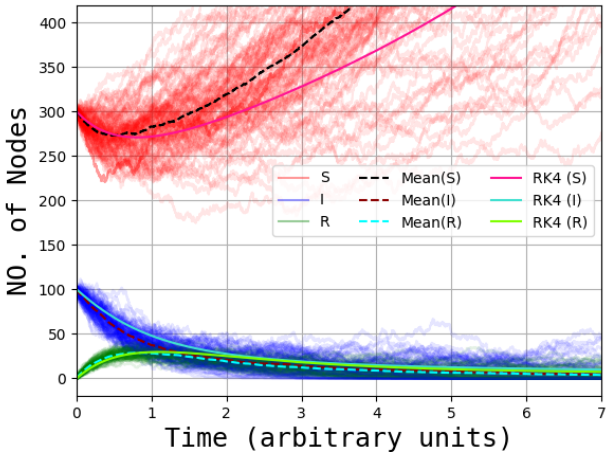

(d) $\alpha = 4$, $\beta = 1$, $\gamma = 0.5$, $\mu = 1$, $\mu^* = 2$, $\epsilon = 1.2$

Figure 5: Temporal development of the S, I and R populations, with vital dynamics modelled.

Figure 5 have the SIR-models with vital dynamics enabled. The variables μ, μ^* and ϵ govern the conditions respectively for death from natural causes, death from infection, and the birth rate.

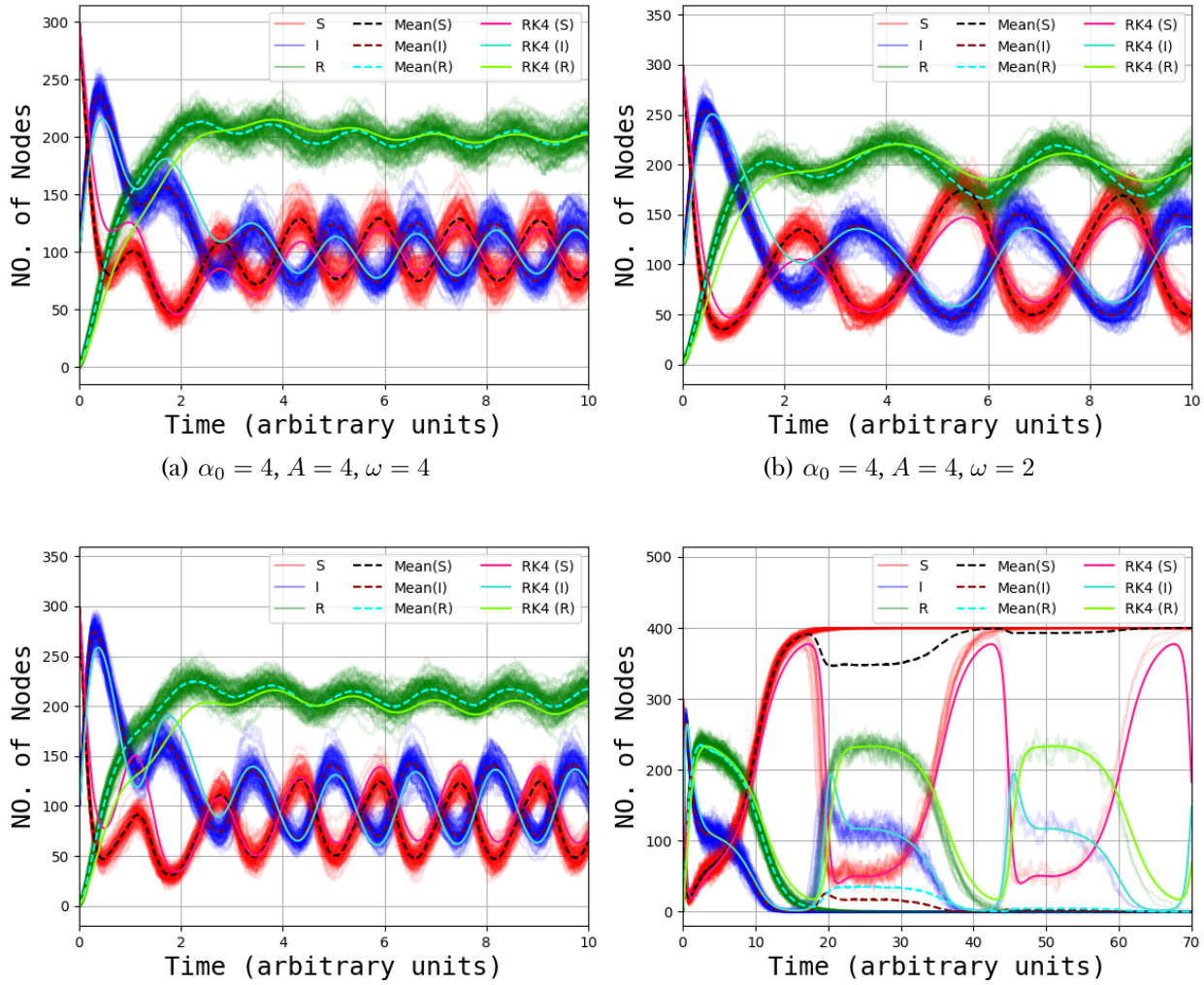

(a) $\alpha_0 = 4$, $A = 4$, $\omega = 4$

(b) $\alpha_0 = 4$, $A = 4$, $\omega = 2$

(c) $\alpha_0 = 4$, $A = 8$, $\omega = 4$

(d) $\alpha_0 = 4$, $A = 4$, $\omega = 0.25$

Figure 6: Development with seasonal variation enabled. Different values for A and ω have been used.

Figure 6 displays four different simulations of the spread of disease in a network where we enable seasonal variation in the rate of infection, $\alpha(t)$.

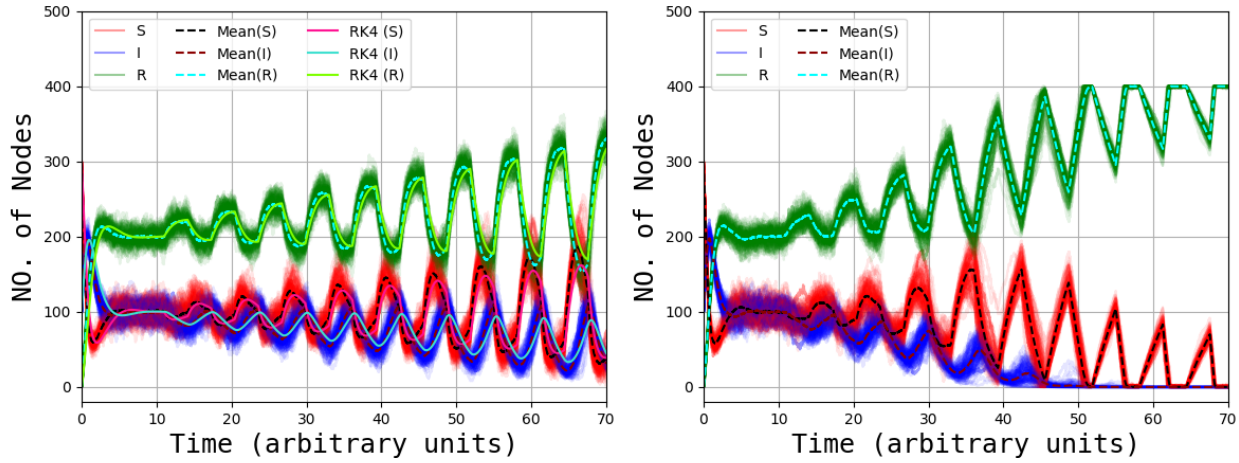

(a) Pulse vaccination, constant γ

(b) Pulse vaccination, variable γ

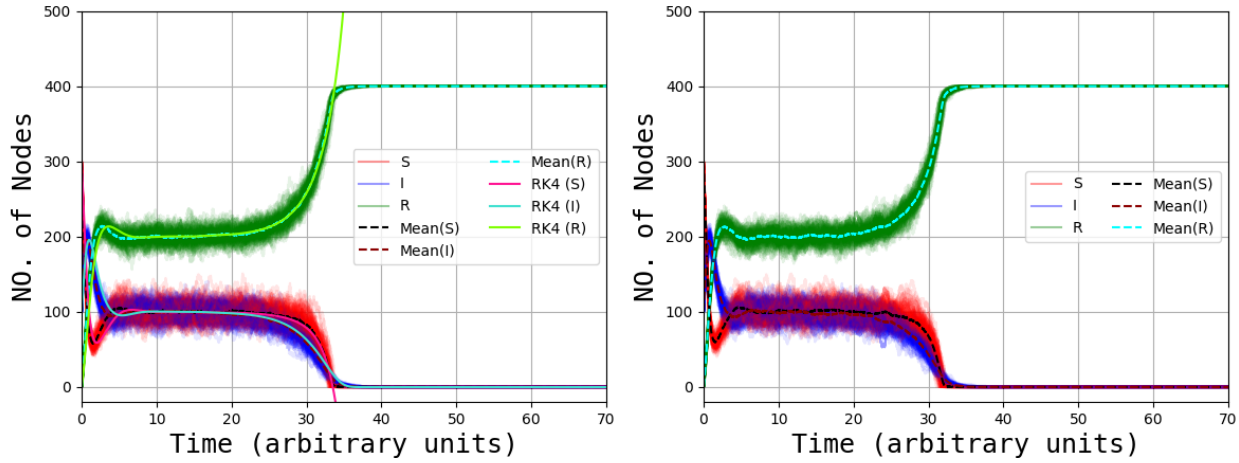

(c) Exponential vaccination, constant γ

(d) Exponential vaccination, variable γ

Figure 7: Development with vaccination with $\alpha = 4$, $\beta = 1$, $\gamma = 0.5$ after time 10 for a and b and after time 15 for c and d

Figure 7 displays the results obtained for simulations in which different vaccination programs are initiated after a given time t. In Figure 7 (b) we have implemented a function which decreases the rate of recovery γ as discussed in Section 4.2.2, and the same was done in Figure 4.2.2. In these plots the ODE solutions are not included as the variable rate of recovery was never implemented for this solver.

6 Discussion

In this numerical project, we have undertaken the task of gradually imposing layers of realism in the SIRS model. Before changing the model at all, we obtain results which may be seen in Figure 4 and Tables 3

and 4. These act at a first glance as a comparison between the deterministic and stochastic approach to simulating the spread of disease in a network. Most notably, the tabulated number of agents occupying each compartment at equilibrium in Table 3 allows for a more detailed comparison between the two. We may observe here that for $\beta = 3$, the expected number of agents in S at equilibrium approaches 400, rather than the theoretical value of 300. Following this deviation, the expected number of infected and recovered agents tend to zero - a very interesting outcome as for a recovery rate that is lower than the infection rate, one would expect the disease to remain within the population at a non-zero equilibrium. For $\beta = 4$, the trend for both the deterministic and stochastic solution is that the total occupation of I tends to zero, i.e. the disease is autonomously eradicated as expected. Concerning the tabulated data, we may also notice that for $\beta = 2, 3$ the standard deviation in the data representing the total number of occupants in each compartment at equilibrium increases dramatically compared to the standard deviation in simulations devising $\beta = 1, 4$. These large deviations are also easily recognized on the plots where there are a wide range of trajectories undertaken in the different simulations. We believe this has to do with the non-linearity of the system. If we turn our attention to Figure 5, the large deviations become even more pronounced when adding terms in the non-linear system, leading us to believe that this is the main reason for the increasing standard deviations. Plots of the temporally evolving standard deviation may be found in Appendix B.

The results obtained from adding the realization of vital dynamics are displayed in Figure 5. This simple improvement alone changes the evolution of disease contagion within a network dramatically. In Figure 5 (a), the birth rate and death rate are set to be equal, and the death rate due to infection is held at zero. As there are more possible transitions into the state of having died, than there are possibilities of being born or 'added' into the network, this simulation tends to zero for all three compartments eventually. However, here we wanted to show that for societies with an insignificant, yet slightly negative population growth, the occupation of I equilibrates at a level which is approximately 20% higher than for the same simulation without vital dynamics within the first 10 time units. Figure 5 (b) simulates a situation in which the infectious disease has a high mortality rate, here set to be equal to both the birth - and death rate. Here we see that in the first time units, the likelihood of dying, whether from natural causes or the disease, is very high. This leads to a rapid fall in the total population. After some time, all agents in the network occupy S, and therefore, the addition and subtraction of agents are in equilibrium as $P(B \to S) = P(S \to D)$ such that the system sets at a non - zero value. More importantly, this only occurs in the stochastic simulation, as the ODE solver suggests that the network size tends to zero after

approximately 30 time units. In Figures 5 (c) and (d), the same process as for (b) occurs, but now we simulate a network in which the population growth is positive.

With seasonal variation added to the model, the rate of transmission α varies periodically with respect to time, and the trends in transitions in the network can be seen in Figure 6. Figures (a), (b) and (c) shows the effect of varying amplitudes and frequencies in a way one would expect. After equilibrating, the agents in R dominate, and the oscillations caused by the varying rate of transmission is evident. In Figure 6 (d) an interesting equilibrium is reached. The Runge-Kutta solution and the Monte-Carlo expectation values diverge around time step 18. The deterministic solution oscillates periodically with areas of extremely high rates of susceptible agents and very few infected agents, before the contaigon flares up again. For the stochastic simulation, there appears to be two variations. One where it follows the deterministic simulation, and one where the number of agents who are susceptible reaches the network size, and the infection is eradicated. As can also be seen, at the high points of S, the stochastic solution will either follow the path to eradicate the contaigon, or follow the deterministic path and have a relapse in infection. At the next high point, the stochastic solution can make this choice of path once more. This shows in a pretty way the advantage a random sampling stochastic solution has over a deterministic one. In real life, there will always be an element of randomness and uncertainty, because of the impossibility of knowing absolutely all variables associated with change. With the Monte Carlo simulations, we are able to mimic the randomness of reality somewhat closer than we are with the Runge-Kutta simulations.

The last plots included in the Results section describe the effect of vaccinating susceptible agents, as to break the cyclic nature of the SIRS model by directly moving them from S to R. As we can see from Figure 7 (c) and (d), had there been a possibility of continuously vaccinating the agents in S, this would lead to a eradication of the disease within a short period of time. However, as this vaccination program is less than economically feasible in many countries, we may rather turn our attention to Figures 7 (a) and (b) as these describe the implementation of a more realistic pulse vaccination program. In simulation (a) we kept γ constant, leading to the issue that vaccinated agents may transition back into S. In (b), however, we used the method described in Section 4.2.2 in order to better ensure that R - occupants do not leave the compartment when already vaccinated. The vaccination function used in these simulations was

$$f(t) \begin{cases} 2t, \text{ if } \cos(t) > 0 \\ 0, \text{ else} \end{cases}$$

as to simulate a pulse with linearly increasing value. Here we wanted to capture a situation in which susceptible agents are vaccinated on regular intervals, but in each interval the availability of the vaccine increases. A plot of the same simulation where the rate of vaccination is a constant percentage of the current number of occupants of S at each interval is included in Appendix C. The effect of pulse vaccination are clear from the presented plots. In the intervals where susceptible agents are vaccinated, the number of infected agents fall dramatically, and as the likelihood of transitioning back into S becomes smaller after each period of vaccination, the next maximum in the infected data will be smaller than the previous one. As a consequence, the number of infected agents steadily decreases in an oscillatory fashion, until it reaches zero. In Figure 7 (b), at approximately 48 time units, the data represented in a light blue hue indicates that in some simulations the disease flares even after the number of infected agents reaches zero. This is a common feature in pulse vaccination, in which there are effectively disease free periods, right before a 'freak' outbreak which is quickly eradicated. This phenomenon is more so visible in Figure 8 in Appendix A. It should also be noted that, even though the latter vaccination program is more realistic, an important difference emerges when comparing the two. The results for a network in which the exponentially increasing rate of vaccination is implemented tends to a disease free equilibrium much faster than for the network dictated by pulse vaccination, leading up to the fact that higher rates of vaccination has a higher likelihood of eradicating a communicable disease. This stresses the idea of mass participation in vaccination programs in order to achieve so-called herd immunity.

Up until this point we have presented select results from our studies of the SIRS model. Although these results serve the purpose of highlighting key findings about the effects of additional realizations to our model, we wish to emphasize that the SIRS model is severely flawed by assuming that the network and the agents it contains mixes homogeneously. In reality, the heterogeneous mixing of a network plays an important role in determining how an infectious disease spreads. Some agents may contact the disease more frequently than others, some may by chance never contact the disease within a given time period. On top of this, the SIRS model fails to further propagate the idea of individuality on a more complex level. Especially for simulations of populations containing sentient human beings, a highly realistic model should take rational behaviour into account. Some people have lower propensity towards being vaccinated or having their children vaccinated, some are more likely to sustain a higher level of

personal hygiene, and a select few might even choose to commit to self-isolation. A major improvement on the SIRS model would be to devise it in conjunction with a spatial model[5], as well as object orienting our code in order to initialize nodes on a spatial grid with different health status IDs.

7 Conclusive Remarks

The SIRS model is an excellent choice for heuristically studying how an infectious disease spreads within a network on the temporal dimension alone. From our select results, it has become clear that both the deterministic and stochastic model approaches to simulating such networks are in every way valid, although the stochastic approach produce results which capture the random nature of such processes in a more organic way, and that are statistically more realistic. It predicts outcomes which deviate from what may be produced by solving a set of differential equations deterministically, which in turn may be analysed in detail. We have added different realizations in our model, such as seasonal variation in the rate of transmission, vital dynamics and vaccination programs, finally arriving at a compound model for even more realistic simulations. Upon the addition of new layers, we are able to get new insight into the essential mechanics of disease spread. Most notably we find that for diseases with high mortality rates, the compartment containing susceptible agents eventually equilibrates at a non-zero level, whilst the two other compartments reaches equilibria containing no agents. Furthermore, in the case of vaccination, we find that vaccinating the agents at a higher rate leads to a much faster tendency towards zero in the infected compartment, which is what we would expect. As to what concerns the performance of our program, we have made some summary remarks on the inherent flaws in the SIRS model we have devised. We have concluded that conjoining the temporal SIRS model with a spatial diffusion model (as an example) will allow for more realistic simulations of the process of disease spread. Object orienting our code will also be helpful in tracking the health status of all of the initialized agents, and is a task that lies ahead of us in our academic career.

[5] In general a diffusion model is used.

A Additional Results

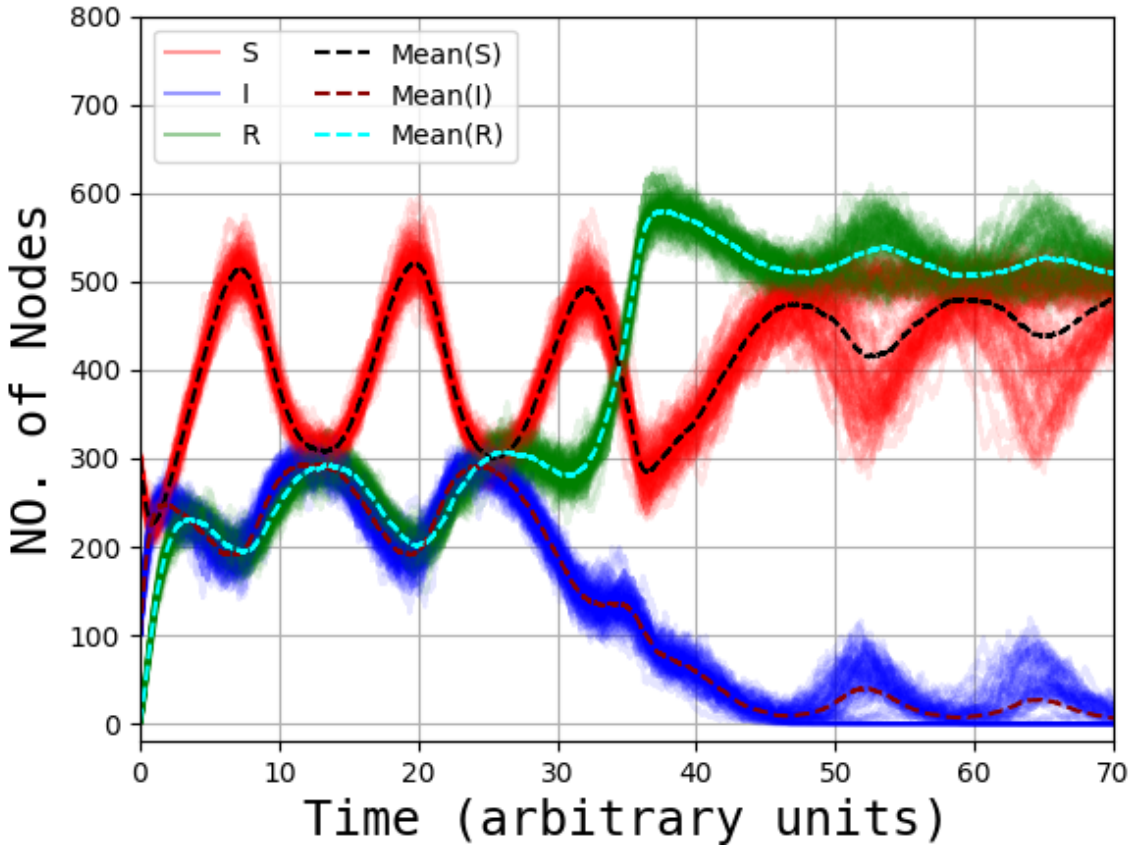

Figure 8: Combination of all additional improvements with $\alpha_0 = 4$, $A = 1$, $\omega = 0.5$, $d = 0.5$, $d_I = 0.2$, $e = 1$ and with exponential vaccination

Figure 8 shows how the total number of occupants in all compartments S, I and R evolves for a compound model including vital dynamics, seasonal variation and exponentially increasing vaccination rates. Notice the disease free intervals after 40 units of time.

B Standard Deviation Plots for Figures 4 a,b,c and d

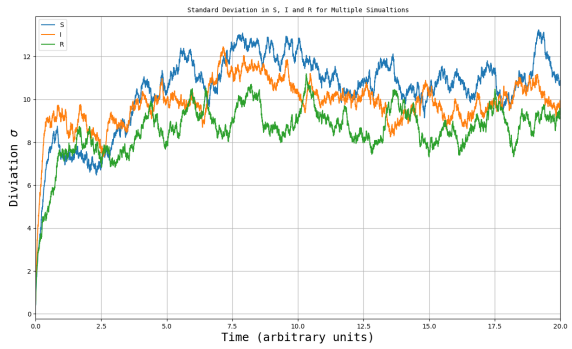

(a) $\beta = 1$

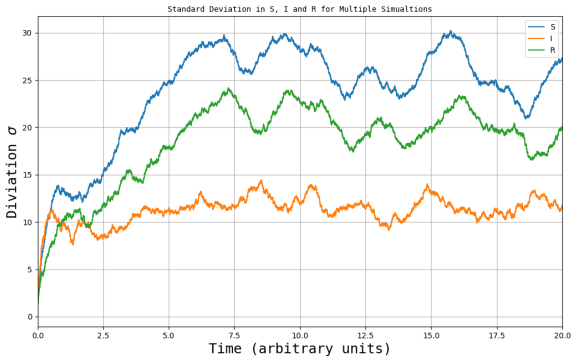

(b) $\beta = 2$

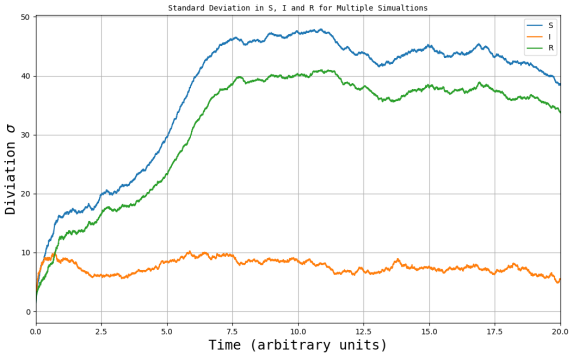

(c) $\beta = 3$

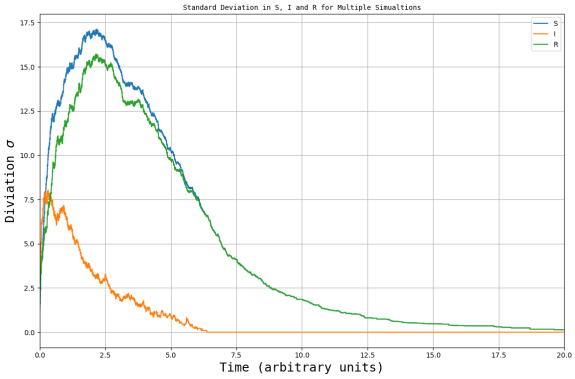

(d) $\beta = 4$

Figure 9: Standard deviation plots belonging to Figure 4, with different initial value for β, the rate of recovery. $\alpha = 4$ and $\gamma = 0.5$

Figure 9 shows the temporal evolution in the standard deviation in the stochastic simulations for the different networks A,B,C and D.

C Pulse Vaccination of a Constant Percentage of the Network

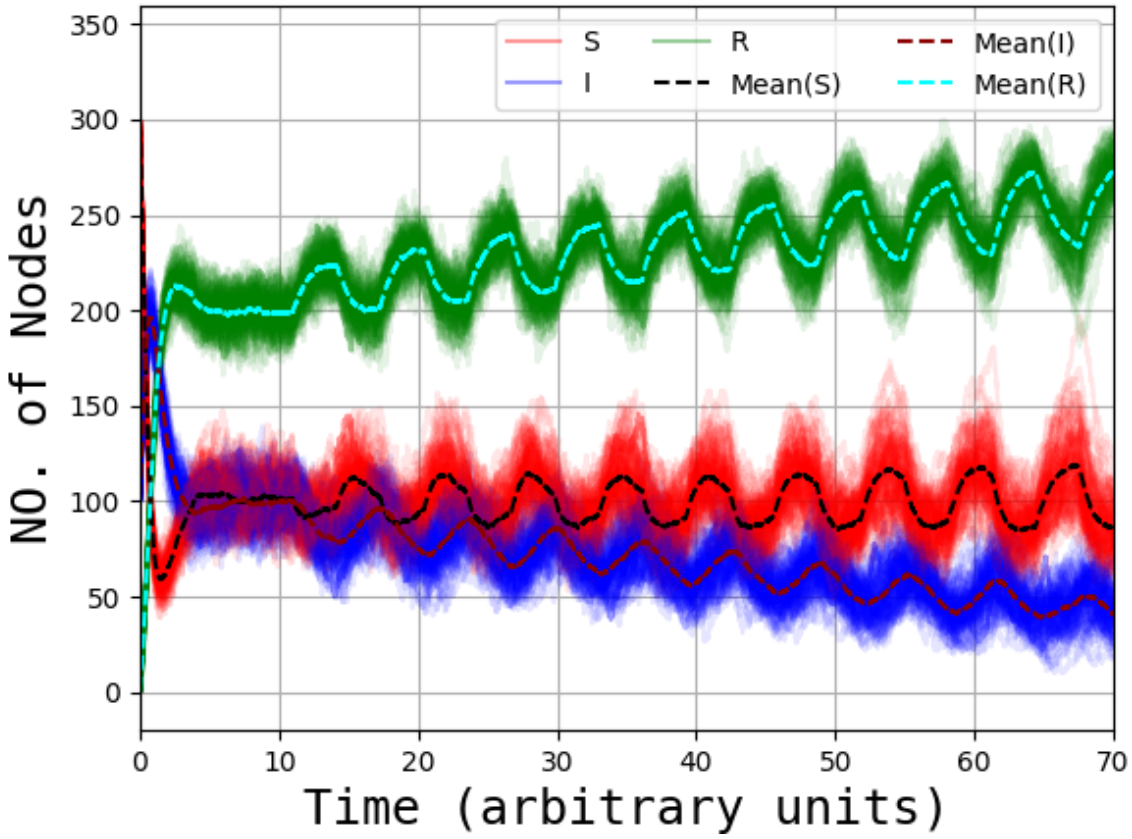

Figure 10: Vaccination with 25% of population in S being vaccinated and variable γ, $\alpha = 4$, $\beta = 1$

Figure (10) is a simulation in which a fraction of the susceptible agents are vaccinated after $t = 10$ at regular intervals. The effects are obvious.

References

[1] Weiss, H. (2013). The SIR model and the Foundations of Public Health. MATerials MATemàtics, Volum 2013, treball no. 3, 17 pp. ISSN: 1887-1097. http://mat.uab.cat/matmat_antiga/PDFv2013/v2013n03.pdf

[2] Berrang-Ford, L., Odiit, M., Maiso, F., Waltner-Toews, D., McDermott, J. (2006). *Sleeping sickness in Uganda: revisiting current and historical distributions. African health sciences*, 6(4), 223–231. https://doi.org/10.5555/afhs.2006.6.4.223

[3] Huremović D. (2019). Brief History of Pandemics (Pandemics Throughout History). *Psychiatry of Pandemics: A Mental Health Response to Infection Outbreak*, 7–35. https://doi.org/10.1007/978-3-030-15346-5_2

[4] Grassly, N. C., Fraser, C. (2006). Seasonal infectious disease epidemiology.*Proceedings. Biological sciences*, 273(1600), 2541–2550. https://doi.org/10.1098/rspb.2006.3604

[5] Fares A. (2013). Factors influencing the seasonal patterns of infectious diseases. *International journal of preventive medicine*, 4(2), 128–132. https://www.ncbi.nlm.nih.gov/pmc/articles/PMC1634916/